Magn Reson Mater Phy (2010) 23:53–64
DOI 10.1007/s10334-009-0194-y

RESEARCH ARTICLE

Detection of vascular alterations by in vivo magnetic resonance angiography and histology in APP/PS1 mouse model of Alzheimer's disease

Nadine El Tannir El Tayara · Benoît Delatour · Andreas Volk · Marc Dhenain

Received: 17 April 2009 / Revised: 3 December 2009 / Accepted: 9 December 2009 / Published online: 12 January 2010
© ESMRMB 2010

Abstract
Object The brain of patients with Alzheimer's disease (AD) is characterized by the presence of amyloid plaques and neurofibrillary tangles. Vascular alterations such as amyloid angiopathy are also commonly reported in patients with AD and participate in mechanisms involved in disease onset and progression. Transgenic mouse models of AD have been engineered to evaluate the pathophysiology and new treatments of the disease. Our study evaluated vascular alterations in $APP_{SweLon}/PS1_{M146L}$ mouse model of AD.
Materials and methods Histological analysis and in vivo magnetic resonance angiography protocols based on time of flight (TOF) and contrast-enhanced (CE) angiography were applied to evaluate cerebrovascular alterations.
Results Histological analysis showed that cerebrovascular amyloid deposition starts by the same time as extracellular amyloid plaques. However, unlike plaques deposition, severity of cerebrovascular alterations is stabilized in older animals. Alteration of the middle cerebral artery was detected in old $APP_{SweLon}/PS1_{M146L}$ mice with respect to adult ones by evaluating the severity of vessel voids and the reduction of vessel length on TOF- and CE-angiograms. Age-related alterations in control PS1 mice were only detected as a reduced vessel length on CE-angiograms.
Conclusion These results show that macroscopic vascular abnormalities are part of the pathological alterations developed by $APP_{SweLon}/PS1_{M146L}$ mouse models of AD.

Keywords Alzheimer's disease · Vascular alterations · Angiography · Angiopathy · Transgenic mouse

N. El Tannir El Tayara (✉) · A. Volk · M. Dhenain
Institut Curie, Centre de Recherche, Orsay, France
e-mail: Nadine.El-Tayara@curie.fr

N. El Tannir El Tayara · A. Volk · M. Dhenain
INSERM U 759, Orsay, France

B. Delatour
CNRS UMR 8620, Laboratoire NAMC, Orsay, France

M. Dhenain
CEA, DSV, I2BM, MIRCen, Fontenay-aux-Roses, France

M. Dhenain
CNRS, URA 2210, Fontenay-aux-Roses, France

Present Address:
B. Delatour
CNRS UMR 7225, CRICM, Paris, France

Introduction

Alzheimer's disease (AD) is a severe and progressive dementia characterized by two main neuropathological lesions: senile plaques and neurofibrillary tangles. Senile plaques are mainly constituted of amyloid-β (Aβ) proteins that aggregate in the extracellular space. Amyloid-β, which is currently considered as a primary drug target for AD treatment, also deposits in the brain vasculature leading to cerebral amyloid angiopathy (CAA), a lesion that is detected in 90% of patients with AD [1].

Parenchymal (plaques) and vascular (CAA) deposition of Aβ do seem to be dependent phenomena. Following its formation, presumably in neuronal cells, Aβ can be transported to the blood vessels where it induces CAA. During AD (and also aging) vascular anomalies can impede Aβ drainage, therefore promoting CAA [2], which in turn might provoke, in a vicious cycle, additional vascular lesions. Many risk factors for AD, such as stroke, hypertension, diabetes, atherosclerosis, and hypercholesterolemia are indeed directly associated with the vascular system [3]. These epidemiological evidences combined with experimental support from

correlative neuropathology, neuroimaging and clinical medicine strengthen the contention that AD and neurovascular disorders are intermingled [4]. The assumption that AD is a subtype of vascular dementia has even been proposed. In addition, many patients with AD display stigmata that suggest vascular alterations [3]. For example, they present with blood flow impairments [5,6] and angiogram alterations [7]. In many cases, vascular alterations have severe consequences in patients as they can lead to cortical hemorrhages, infarctions, and severe lobar cerebral hemorrhages (see [8] for review). Being able to detect and cure vascular alterations is thus critical to prevent premature death/dementia of the patients and therefore to improve the prognosis of the disease.

Transgenic mouse models developing cerebral amyloidosis have been engineered to evaluate the pathophysiology and new treatments of AD [9]. They are based on the overexpression of mutated forms of the amyloid β precursor protein (AβPP), possibly associated to the overexpression of mutated forms of presenilins (PS1 or PS2). These models display extracellular amyloid deposits and various degrees of CAA [10,11]. Many studies focused on pathophysiological events related to parenchymal amyloid plaques. Vascular impairments are however also important parameters to evaluate in these models, given the vascular alterations described in human patients with AD. Ideally, such impairments should be evaluated by histology but also by in vivo protocols that might help to follow-up the effect of experimental therapeutics.

We have previously evaluated pathological alterations associated to the overexpression of human mutated AβPP and PS1 in the $APP_{SweLon}/PS1_{M146L}$ (APP/PS1) mouse model of AD. This model is relatively aggressive as extracellular amyloid deposition starts at the age of 2.5 months [12]. Mice show brain atrophy but it involves mainly white matter tracts rather than cortical regions [13]. Until now, vascular alterations have not been studied in this transgenic line. The aim of our study was thus to evaluate cerebrovascular alterations in APP/PS1 mice by concurrent histological and *in vivo* imaging approaches. Among imaging techniques that provide global architecture of the cerebrovasculature, magnetic resonance angiography (MRA) is a non-invasive method that proved its value in depicting cerebrovascular abnormalities in patients with AD [7] and in mice [14]. This method was thus selected to assess cerebrovascular abnormalities in APP/PS1 mice.

MRA can be realized by phase contrast (PC-MRA), time of flight (TOF) as well as contrast enhanced (CE-MRA) techniques. TOF-MRA is commonly used to evaluate artery angiograms in rats [15] or mice [16,17]. This technique exploits the inflow of water protons at thermodynamic equilibrium inside the vessels to generate high contrast with respect to residual signal from saturated water protons in stationary tissue. CE-MRA is based on the injection of a paramagnetic contrast agent. In CE-MRA, intravascular signal is increased by shortening the T1 relaxation time within the vessels, independently from inflow effects. This method provides morphological information concerning arteries as well as veins and may allow visualization of arteries which are not detected on TOF-angiograms due to low flow rates. Consequently, both TOF- and CE-MRA techniques were used in our study to evaluate cerebrovascular alterations in APP/PS1 mice.

In the present study, histological assessment showed that APP/PS1 mice modeling AD develop CAA in addition to parenchymal plaques. The kinetics of these vascular and parenchymal amyloid deposits were further assessed. In APP/PS1 mice, age-related morphological and presumably functional alterations of the middle cerebral artery (MCA) were detected, in vivo, by TOF- and CE-MRA.

Materials and methods

Animals

Our experiments involved $APP_{SweLon}/PS1_{M146L}$ mice modeling Alzheimer's disease. This transgenic line is based on the over-expression of the human AβPP driven by the thy-1 promoter and harboring three familial mutations (Swedish (K670M/N671L) and London (V717I) mutations). In addition, over-expression of PS1 mutation (M146L) leads to an acceleration of the pathological alteration. These mice display cerebral amyloid deposition at 9–14 weeks of age [12, 18,19]. The $APP_{(+/wt)}/PS1_{(+/wt)}$ mice (APP/PS1) used in this study were obtained by crossing $APP_{(+/wt)}/PS1_{(wt/wt)}$ with $APP_{(wt/wt)}/PS1_{(+/+)}$. Note that, due to the use of homozygous $PS1_{(+/+)}$ mice, no wild-type mice could be generated from the breeding scheme. The $APP_{(wt/wt)}/PS1_{(+/wt)}$ (PS1) mouse littermates were used as controls. These mice do not display any amyloid deposits (no plaques, no CAA) and are thus good controls to evaluate the effects of AβPP on amyloid deposition in the brain [13,20]. For MRI studies, animals were divided into two age groups, "adult" (16–23-week-old animals, 7 APP/PS1 and 7 PS1 mice), and "old" animals (60.5–84.5-week-old, 7 APP/PS1 and 6 PS1 mice). Histological studies involved 24 APP/PS1 mice (17–124 weeks) and 5 PS1 animals (52–111 weeks). All experiments were conducted in accordance with ethical standards of the statutory order 87 848 (October 13, 1987) of the French Ministry of Agriculture (authorizations nos. 91–166 and 91–282).

Histology

Histological analyses were performed to assess amyloid deposits and CAA in APP/PS1 and PS1 mice. First, histological sections from APP/PS1 mice (17–124 weeks, $n = 17$)

and PS1 animals (96 weeks, $n=2$) were stained by Congo red method as previously described [13]. Briefly, following decapitation the brains were extracted, fixed in 10% buffered formalin and then stored overnight in a solution of 20% glycerin and 2% dimethylsulfoxide in 0.1 M phosphate buffer for cryoprotection. Brains were subsequently sectioned into 40 μm-thick coronal sections on a freezing microtome. Then, serial sections ranging from the frontal to the occipital poles were stained. Amyloid deposits in the parenchyma and in cerebral vessels were labeled by standard Congo red staining (30 min in an 80% ethanol solution saturated with congo red and sodium chloride (adapted from [21]). Each slice was then digitized using a Super CoolScan 8000 ED high-resolution scanner (Nikon, Champigny sur Marne, France). Regional amyloid loads (expressed as percent of tissue surface stained by the Congo red dye) were quantified in the parietal, temporal, and occipital cortices, using computer-based thresholding methods as previously described [13]. An index of the global amyloid load in the brain from each mouse was calculated by averaging the amyloid load in these areas.

The severity of CAA was assessed in Congo red-stained sections from parietal, temporal and occipital cortices by using a semiquantitative method based on a four-point scale (Grades 0–3) [22,23]. For each section, a score was attributed according to the following scale: 0 = no staining in small arteries, arterioles or capillaries; 1 = few Congo red–positive leptomeningeal vessels detected; 2 = few leptomeningeal vessels stained but associated with mild intracortical vascular involvement; 3 = many leptomeningeal and intracortical vessels affected. An index of the severity of the CAA in the whole brain from each mouse was calculated by averaging the CAA scores in the parietal, temporal and occipital cortices. To further evaluate angiopathy in cerebral vessels, superficial vessels such as the anterior, middle and posterior cerebral arteries (nAPP/PS1 = 7, age: 31–111 weeks; nPS1 = 3, age: 52, 83 and 111 weeks) were dissected, stained by thioflavin-S and mounted in Mowiol (Calbiochem-Novabiochem, La Jolla, CA) on a glass slide. From original microphotographs, reconstruction of vasculature was performed using AutoStich freeware (Version 2.184, http://www.cs.ubc.ca/_mbrown/mb/mb.html [24]).

Finally, in order to characterize which Aβ species are involved in CAA, we performed anti-Aβ immunohistochemistry (immunoperoxidase method) using dedicated polyclonal antibodies directed against Aβ 1–40 or Aβ 1–42 (FCA-3340 and FCA-3542, VWR, Strasbourg, France). Experiments were performed on two young APPxPS1 mice (23 weeks), three old APPxPS1 mice (>80 weeks) and one old PS1 mouse (96 weeks). Following blocking of endogenous peroxidase activity and of non-specific sites, tissue sections were incubated in primary antibodies (1:5,000, 24 h RT) and then reacted with secondary antibody and avidin–biotin complex. Final reaction made use of diaminobenzidine. Sections were finally counterstained with nuclear fast red (Vector Laboratories, Burlingame, CA, USA).

MRA acquisition protocols

TOF-MRA

In vivo cerebral MRA images were recorded on a 4.7-Tesla Bruker Biospec 47/30 system equipped with a 12 cm diameter gradient system (200 mT/m). For signal acquisition, a surface coil (diameter = 25 mm), actively decoupled from the transmitting birdcage probe (Bruker GmbH) was used. Animals were anesthetized with isoflurane (5% for induction, 1–1.5% for maintenance) in a mixture of N_2(80%) and O_2(20%) administered via a facemask. Respiration rate was monitored to check animal conditions until the end of the experiment. The body temperature of the mice was stabilized by using a heating blanket. MRI protocols were performed on 14 double transgenic APP/PS1 mice that were compared to 13 single transgenic PS1 amyloid-deposit free controls. TOF-MRA were recorded by using a flow compensated 3D gradient echo sequence with the following parameters: repetition time (TR) = 19 ms, echo time (TE) = 3.3 ms, flip angle (α) = 30°, field of view (FOV) = $1.5 \times 2 \times 1.5\,cm^3$, acquisition matrix = $96 \times 128 \times 64$, Number of averages (Nex) = 10, acquisition time 25 min. All data were zero-filled to 128 × 128 × 64.

CE-MRA

In APP/PS1 and PS1 mice, CE-MRA was performed using a "blood pool agent": P792 (Vistarem®, Guerbet, France) [25] at a dose of 45 μmol/kg. The black color of our mice (C57Bl6 background) made the injection in the tail vein very challenging and hardly reproducible; in consequence, all the contrast agent injections were performed in the retro-orbital sinus. CE-MRA was carried out on each mouse systematically after TOF-MRA acquisition (see above; 7 APP/PS1 and 7 PS1 adult mice, and 7 APP/PS1 and 6 PS1 old mice). A volume of 0.1 ml of P792 diluted in NaCl solution was injected within 3 s and acquisition started 2 min after injection. Images were recorded by using a 3D gradient echo sequence with the following parameters: TR = 19 ms, TE = 4.4 ms, α = 30°, FOV = $1.5 \times 2 \times 1.5\,cm^3$, acquisition matrix = $144 \times 192 \times 104$, Nex = 2, acquisition time 12 min 41 s. All data were zero-filled to 256 × 256 × 128. For each angiographic protocol, parameters of acquisition were chosen to optimize image quality. APP/PS1 and PS1 mice studied by MRI were involved in other in vivo imaging protocols and were thus not sacrificed at the end of the experiments.

MRA: Image processing and analysis

Angiogram reconstruction

Several steps were used to reconstruct the angiograms. First, brain tissues were manually extracted using Amira 3.1® software (Mercury Computer Systems, Inc. TGS Unit, Villebon, France). Images of the extracted tissues were then interpolated to a matrix of $256 \times 352 \times 256$ for CE-MRA and to $128 \times 176 \times 128$ for TOF-MRA. Angiograms were then obtained by generating maximum intensity projections (MIPs) from the extracted regions. Blood vessel identification was performed by inspecting the angiograms under various angles and comparing the vessels to anatomical atlases [26,27].

Definition of the vessels displayed in angiograms

Arteries were always visible on TOF- and CE-angiograms. They were classified as (Fig. 1): the azygos anterior cerebral artery (which ascends in a dorsal and slightly caudal direction, becoming the azygos pericallosal artery), gives off the medial orbitofrontal artery from its ventral wall [27]. The anterior cerebral artery (the anterior part of the circle of Willis), the middle cerebral artery (MCA), and the posterior cerebral artery which are terminal branches of the internal carotid artery. The superior cerebellar artery which is a terminal arborization of the basilar artery. The pterygopalatine artery which supplies mostly extracranial structures. This artery enters the tympanic bulba, travels along the medial wall of the tympanic cavity and then emerges intracranially at the angle between tympanic bulba and the petrous bone [27].

Careful examinations of TOF- and CE-angiograms also allowed to identify unusual findings in a subset of mice. The anterior part of the circle of Willis showed sometimes ($n = 2/14$ for APP/PS1, $n = 3/13$ for PS1 mice) 'buttonhole' formations uni- or bilaterally (Fig. 2a). This feature was previously described in the rat cerebrovasculature [27]. In rats, 'buttonhole' formations could extend into the azygos anterior cerebral artery. We also observed (in 2/14 APP/PS1 and 4/13 PS1 mice) an unidentified vessel which started at the level of the circle of Willis and progressed near the posterior cerebral artery (Fig. 2b). This vessel was reported previously [28]. The last anatomical finding was the presence of a uni- or bilateral close contact between the posterior cerebral and the superior cerebellar arteries ($n = 8/14$ for APP/PS1, $n = 5/13$ for PS1), which may correspond to an anastomosis as described in a previously published paper [16] (Fig. 2c, d). These particularities were not considered as pathologic in the following parts of the study.

Assessment of vasculature impairments in APP/PS1 and PS1 mice

Angiograms were analyzed by a method based on the visual evaluation of severity of signal voids within the vessels and by a method that assessed the length of the vessels.

Evaluation of signal voids on cerebral arteries The TOF-angiograms were inspected under various angles by

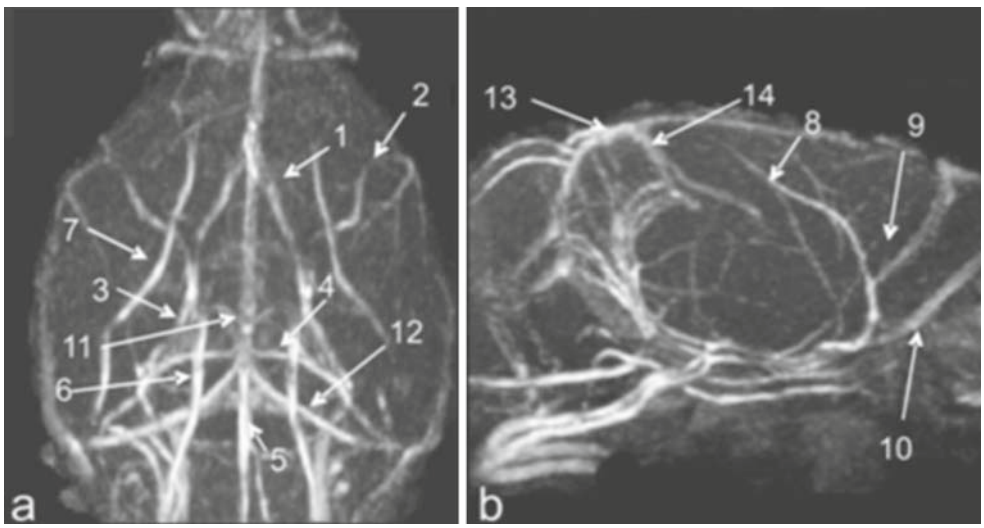

Fig. 1 Identification of blood vessels detected on angiograms (images recorded after the injection of P792 in a 22-week-old APP/PS1 mouse; resolution $59 \times 78 \times 117\ \mu m^3$ after zero filling). Coronal **a** and sagittal **b** projections. The following vessels were detected: arteries: *1*. Anterior cerebral artery (anterior part of the circle of Willis), *2*. Middle cerebral artery (MCA), *3*. Posterior cerebral artery, *4*. Superior cerebellar artery, *5*. Basilar artery, *6*. Internal carotid artery *7*. Pterygopalatine artery, *8*. Azygos pericallosal artery, *9*. Medial orbitofrontal artery, *10*. Olfactory artery; sinuses and veins: *11*. Superior sagittal sinus, *12*. Transverse sinus, *13*. Caudal confluence of sinuses, *14*. Straight sinus

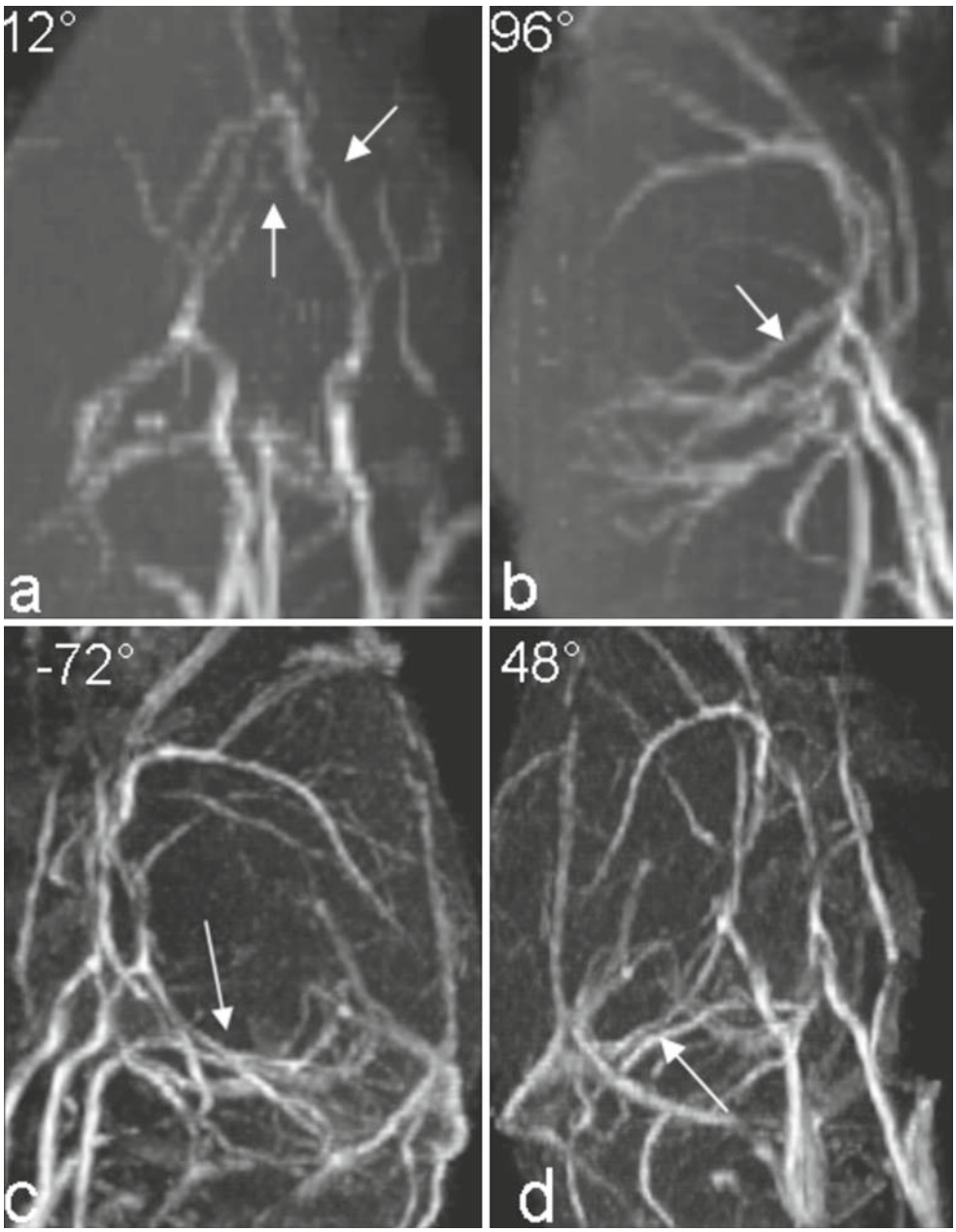

Fig. 2 Unusual anatomical findings detected on TOF and CE-angiograms. **a** Bilateral 'buttonhole' formations detected at the level of the anterior cerebral artery (*arrows*), TOF angiogram of a 84-week-old APP/PS1 mouse. **b** Unclearly identified vessel (*arrow*) starting at the level of the circle of Willis and progressing near the posterior cerebral artery (same angiogram as in **a**). **c** A close contact between the posterior cerebral artery and the superior cerebellar artery (angiogram of a 22-week-old APP/PS1 mouse acquired after injection of P792). This close contact was observed whatever the projection angle. **d** On the other side of the brain, this close contact between arteries was not observed (same angiogram as in **c**). Projection angles are given with respect to the coronal projection

using 3D visualization software (Paravision 3 (Bruker GmbH)). We evaluated the severity of signal voids within all cerebral arteries previously identified. Each vessel was graded on the basis of the number and extents of signal voids detected on MR angiograms. A signal void was counted when the signal intensity at the level of a blood vessel reached background level. The analysis was performed by an experimentalist who was blind to the animal genotypes. The grades were defined as follows: (1) continuous apparent vessel shape, i.e. a vessel that had a non-altered shape (see the MCA in Fig. 3a), (2) one or two focal signal voids: a focal signal void was defined as a void which length was at most twice the diameter of the vessel (see arrow head at the level of the MCA in Fig. 3b), (3) one extended signal void: an extended void was defined as a void longer than a focal void (see arrows at the level of the MCA in Fig. 3b). (4) more than two focal

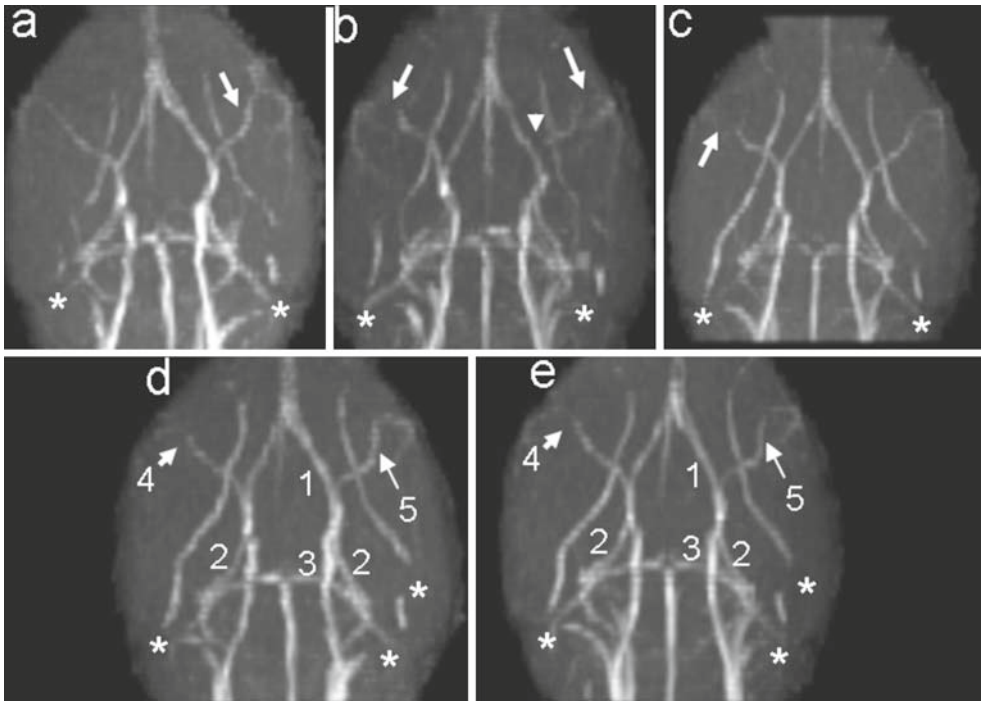

Fig. 3 Examples of various severities of alterations found on TOF-angiograms. **a** Angiogram of an adult PS1 mouse showing a continuous shape of the MCA (*arrow*): The attributed score was 1 for this artery. **b** Angiogram of an old APP/PS1 mouse. The MCA on the right side showed both a focal signal void (*arrow head*) and an extended signal void (*arrow*). Such alteration was scored 4. The MCA on the left side showed only one extended signal void (*arrow*) and was scored 3. **c** Angiogram of an adult APP/PS1 mouse in which the distal part of the MCA on the left side was not detected (*arrow*). This alteration was scored 5. On the other side, the MCA was not altered. Note that the pterygopalatine artery was altered in all animals (*asterisks*). **d–e** Angiograms of the same APP/PS1 mouse recorded on subsequent days (*n* and $n+2$) showing the good reproducibility of angiograms. Both angiograms showed non-altered circle of Willis *1*, posterior cerebral artery *2*, superior cerebellar artery *3*. On the left side, the same alteration pattern of the MCA *4* was detected. MCA were not altered on the right side *5*. Note that at the level of the pterygopalatine artery (*asterisks*), both angiograms showed also the same alteration pattern

or a combination of localized and extended signal voids, (5) total or partial absence of the vessel (compare left and right side of the MCA in Fig. 3c). The absence of a vessel was validated when the vessel was not visible under any possible angle of inspection.

As the MCA was the most altered vessel on TOF-angiograms (see results), we focused on this artery and graded its alterations after the injection of P792 contrast agent by using the same grading scale as on TOF-angiograms.

Evaluation of the length of the vessels The lengths of the MCA, posterior cerebral artery, and circle of Willis were quantified on TOF-angiograms using the software ImageJ (NIH, USA) with the following steps (Fig. 4). First, a region of interest (ROI) was outlined around each vessel. Second, background signal level (S) was assessed in a second ROI on the background cerebral tissue and a threshold corresponding to $S+(0.2 \times S)$ was calculated. Pixels within the ROI surrounding the vessels were segmented to select pixels with a signal superior to the calculated threshold. Finally, the segmented pixels were skeletonized. The length of these skeletonized pixels was used as an index of the length of the vessels. These measurements were performed on the coronal projection of the angiograms for all animals.

As TOF-angiograms revealed differences only in MCA's length between adult and aged APP/PS1 (see results), we only measured the length of this artery on CE-angiograms.

Statistical analysis

Statistical analyses were based on the stringent non-parametric tests of Mann–Whitney and Wilcoxon (Statistica 5, StatSoft, Inc., Tulsa, USA). The statistical significance level was set to a p value <0.05.

Results

Angiogram alterations

Alterations detected on TOF-angiograms

First, we assessed signal voids on vessel paths. In both genotypes, these voids were mainly detected at the level of the

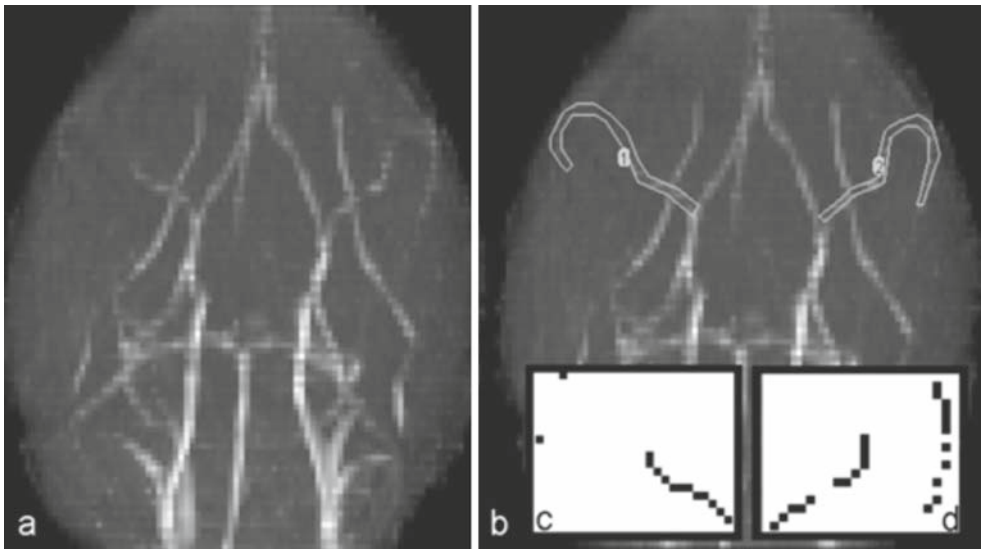

Fig. 4 **a** Angiogram of an APP/PS1 mouse showing alterations at the level of the MCA. **b** ROIs traced on the MCA. **c** and **d** skeletonization of the MCA. Only pixels of the vessel with signal intensity greater than 1.2 times the background tissue signal level were taken into consideration in the skeletonization of the vessel and in the evaluation of its length

MCA and of the pterygo part of the pterygopalatine artery. The latter alterations occurred in all mice (Fig. 3). They were probably caused by susceptibility effects due to the presence of the tympanic bulba in this region [27]. On the contrary, alterations of the MCA were detected only in some animals. Figure 3b shows an example of signal voids at the level of the MCA in an old APP/PS1 mouse. Figure 3c shows also a more critical type of alteration where the whole distal part of the MCA was not detected. Other arteries such as the anterior and posterior cerebral arteries as well as the superior cerebellar artery showed only rarely signal voids whatever the mouse genotype. Some other arteries such as the azygos anterior cerebral artery and the azygos pericallosal artery never showed any alteration in TOF-angiograms from both APP/PS1 and PS1 mice.

Once the possible alterations of the vessels were identified, we checked the reproducibility of the angiographic method by recording angiograms of the same mice at two days of interval. Angiograms of the same mice recorded twice were very similar and showed the same alteration patterns (Fig. 3d, e). Following this control, the severity of the vascular lesions was quantified. The MCA of aged APP/PS1 mice had higher scores for signal voids than adult APP/PS1 mice ($U=7$; $p<0.05$, Fig. 5a). This was not the case in PS1 animals (Us = 16.5; ns). Also, in APP/PS1 but not in PS1 mice, the MCA was shorter by 27% in old mice when compared to adult ones ($U=3.5$, $p<0.05$, Fig. 5c). No significant difference between age-matched PS1 and APP/PS1 mice could be detected when we evaluated the severity of signal voids ($U>12$; ns) or the length of the MCA ($U>14$, ns).

For the other studied vessels, no significant difference between animal groups (APP/PS1 vs. PS1; "adult" vs. "old" mice) was detected concerning the severity of signal voids ($U>10$; ns) or the length of the vessels ($U>10$; ns).

Alterations detected on CE-angiograms

The P792-enhanced angiograms allowed to detect veins (the superior sagittal sinus, the transverse sinus, and the straight sinus (Fig. 1)). As on TOF-angiograms, most of the signal voids were detected at the level of the MCA (data not shown). Other arteries (the anterior, azygos pericallosal, posterior cerebral and superior cerebellar arteries) and sinuses (sagittal, transverse and straight sinuses) showed little to no alterations (data not shown). When a signal void was detected on TOF-angiograms, it was most often also seen on CE-angiograms. This was the case in 77% of the detected voids on TOF-angiograms in APP/PS1 mice, as well as in PS1 mice.

As age-related alterations were detected at the level of the MCA on TOF-angiograms of APP/PS1 mice, we focused on this artery on CE-MRA. First, for each genotype and age group, we noticed that the measured length of this artery was greater on CE- than on TOF- angiograms (Wilcoxon's test, $p<0.05$; Figs. 5c, d, 6). As on TOF-angiograms, scores reflecting the severity of signal voids within the MCA were significantly higher in old APP/PS1 mice with respect to adult ones ($U=7.5$; $p<0.05$; Fig. 5b). Also, the MCA was shorter in old APP/PS1 by 26% when compared to adult mice ($U=7$, $p<0.05$ (Fig. 5d)). In PS1 mice, the severity of signal voids was similar in adult and old animals ($U=11$; ns), while the length of the MCA was reduced by 31% in old animals when compared to adult ones ($U=5$, $p<0.05$ (Fig. 5d)). No significant difference between age-matched

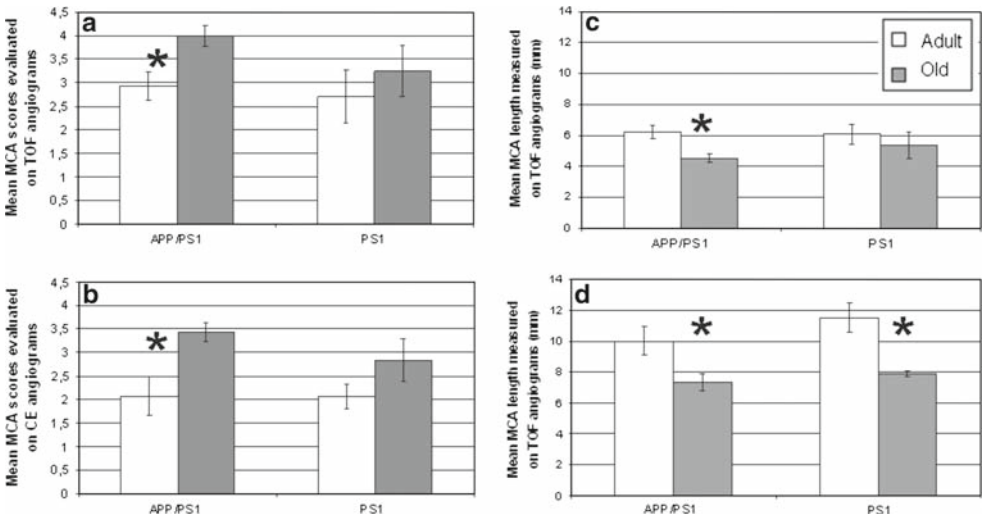

Fig. 5 **a** and **b** Mean scores attributed to evaluate alterations of the MCA on TOF- and CE-angiograms respectively. **c** and **d** Mean length of the MCA detected on TOF- and CE-angiograms respectively. "Adult" mice: 16–23 weeks of age (7 APP/PS1 and 7 PS1 mice); "old" animals: 60.5–84.5 weeks of age (7 APP/PS1 and 6 PS1 mice); *: $p<0.05$

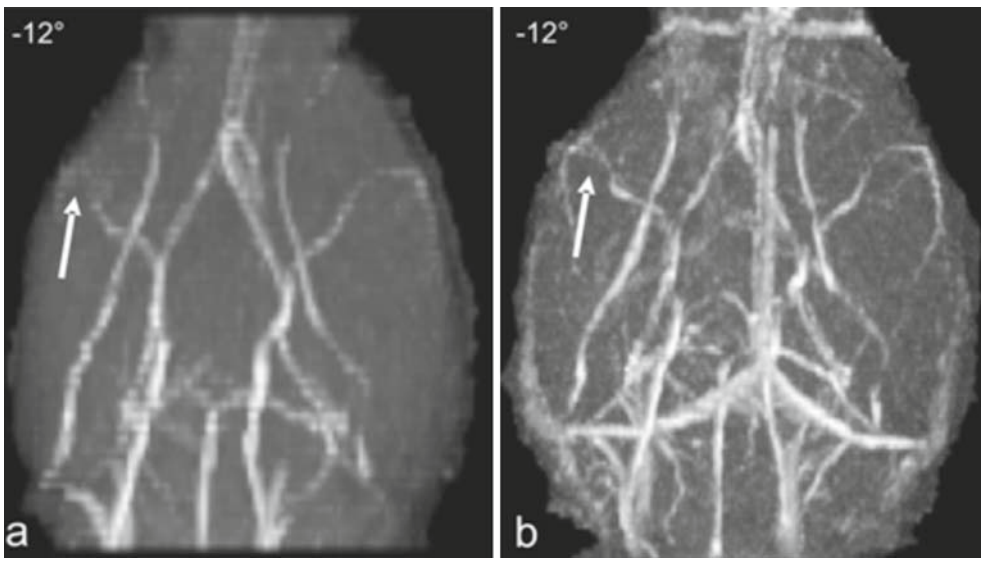

Fig. 6 Angiograms from an APP/PS1 mouse before (**a**) and after the injection of P792 (**b**). The detected MCA was longer on CE-MRA than on TOF-MRA. Particularly, on the left side of the images, the distal part of the MCA 'truncated' on the TOF-angiogram (**a**, *arrow*) was detected after injection of P792 (**b**, *arrow*). This suggests that the signal absence detected on the TOF-angiogram was not related to vessel disruption or loss. Projection angles are given with respect to the coronal projection

PS1 and APP/PS1 mice could be detected when we evaluated the severity of signal voids ($U>16$; ns) or the length of the MCA ($U>14$, ns).

Plaques and vascular amyloid depositions in APP/PS1 mice

From the analysis of Congo red sections, it appeared that all studied APP/PS1 animals displayed Aβ plaques. In the youngest animals (age$<$23 weeks), Aβ deposits were only localized in the subiculum (data not shown, but see [29]). With aging, amyloid burden increased steadily and plaque deposition spread out in numerous regions of the brain (Fig. 7a). The topography of amyloid deposits was indeed reminiscent of previously published observations [12]. A linear correlation was observed between age and the cortical amyloid loads ($rs>0.95$, $ps<0.0001$, Fig. 7e). As expected, amyloid plaques were not detected on Congo red sections from PS1 mice.

Congo red-stained sections also revealed CAA in cerebral vessels of APP/PS1 (Fig. 7b, c). CAA was detected in various vessels of the brain (for example the branching of the middle cerebral artery (Fig. 7f) or the small cortical

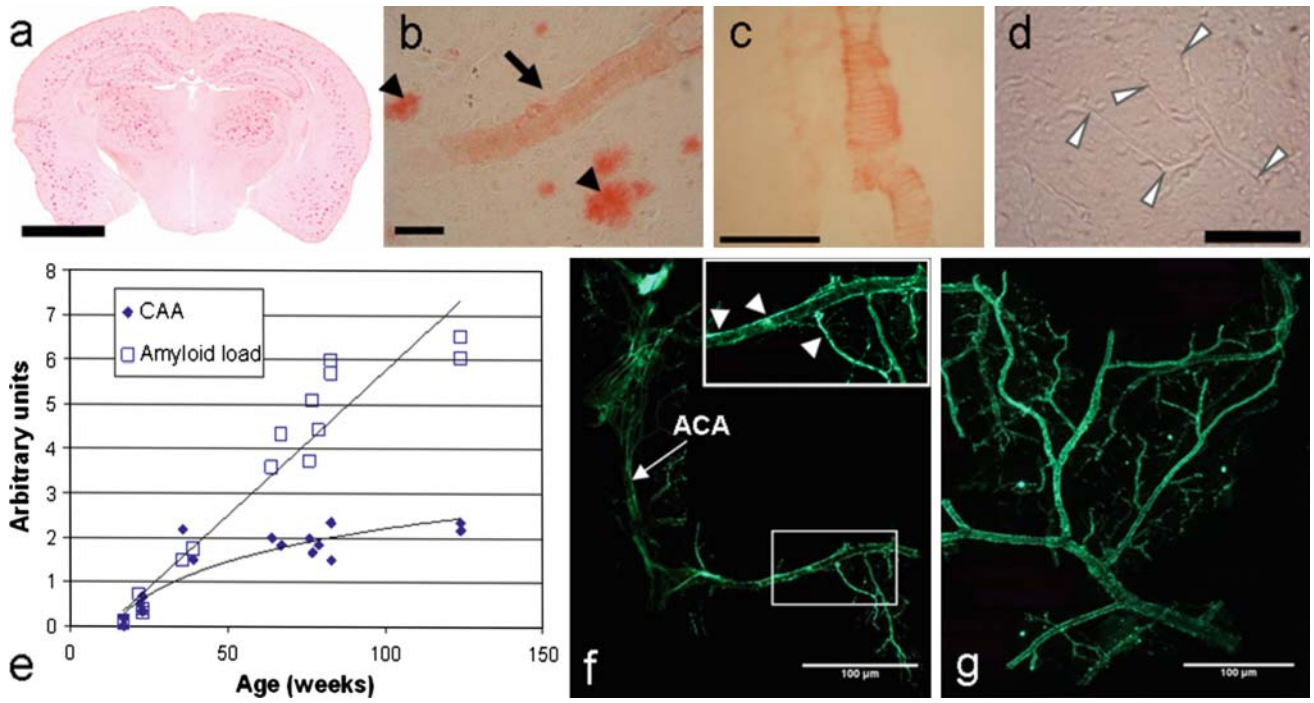

Fig. 7 Congo red staining showing amyloid plaques and CAA in APP/PS1 mice. **a** Amyloid plaques (*red spots*) in a 64-week-old APP/PS1 mouse. **b** CAA detected in a cortical vessel (*arrow*) of a 77-week-old APP/PS1 mouse. Parenchymal plaques are indicated by arrow heads. **c** Portion of the posterior cerebral artery of a 76-week-old APP/PS1 mouse displaying CAA with a pattern of amyloid deposition in concentric rings. Scale bars: 500 µm for **a**, 50 µm for **b** and **c**. **d** Congo red-stained section of a PS1 single transgenic mouse (photograph taken with small diaphragm aperture to increase depth of field and contrast). No amyloid deposits were found in cortical blood vessels of PS1 transgenics (arrow heads point to vessel branches). Scale bar: 50 µm. **e** Age was correlated to the global cortical amyloid load ($y = 0.0652^{*}x - 0.7689$; $r = 0.96$, $p < 0.0001$). The correlation between CAA (global score) and age was better described by a logarithmic curve than by a linear curve ($y = 1.0916^{*}Ln(x) - 2.8204$, $r = 0.9$, $p < 0.0001$) and the severity of CAA seemed to be stabilized beyond 40 weeks. **f, g**: Thioflavin staining: **f** CAA (*arrow heads*) detected in the branches of the MCA extracted from an 80-week-old APP/PS1 mouse. Inset shows higher magnification of the outlined area of the MCA. Note that the anterior cerebral artery (ACA) was devoid of CAA; **g** CAA in cortical vessels from a 103-week-old APP/PS1 mouse. Scale bars: 100 µm for **f** and **g**

vessels (Fig. 7g) by Congo red histochemistry or thioflavin-S staining of isolated vessels.

Some vessels were less affected than others. For example, the anterior cerebral artery was devoid of CAA even in mice displaying severe amyloidosis of the MCA (Fig. 7f). Cerebral amyloid angiopathy was never detected on Congo red sections or thioflavin-stained vessels from PS1 mice (Fig. 7d).

Quantification of CAA from Congo red-stained sections revealed that cortical CAA was already detected in 18-week-old mice (Fig. 7e). The fit of the semiquantitative scoring of CAA severity (in all studied cortices) versus age was more precisely defined by a logarithmic ($rs > 0.81$, $ps < 0.0001$, Fig. 7e) than by a linear regression model ($rs > 0.71$, $ps < 0.01$). The CAA severity seemed to be stabilized beyond the age of 40 weeks. "Old" animals (60.5–84.5 weeks) showed extensive CAA in the cerebrovasculature, while "Adult" mice (16–23 weeks) displayed a low CAA load.

Using immunohistochemistry we observed in both young and old APP × PS1 mice, a very large prevalence of the Aβ40 isoform, forming amyloid deposits in the vascular system but also aggregating in extracellular plaques (Fig. 8). Also, using immunohistochemistry, we did not observe any Aβ 40 nor Aβ 42 positive blood vessels in PS1 mice.

Discussion

We evaluated vascular alterations in a double transgenic $APP_{SweLon}/PS1_{M146L}$ mouse model of AD. APP/PS1 mice were compared to amyloid-free single PS1 transgenics. This allowed us to assess specifically the effect of the AβPP transgene that leads to amyloid deposition in the brain tissue and vasculature.

Our histological study showed that APP/PS1 mice develop CAA in addition to parenchymal amyloid plaques. Immunohistochemical analyses revealed that Aβ deposition in blood vessels (but also in parenchymal plaques) was mainly constituted of the 40 amino acids isoform (see also [30,31] for similar observations in other AD transgenic lines and in patients with AD). Cerebral amyloid angiopathy and amyloid plaques both started to be detected from about 20 weeks of age. In our

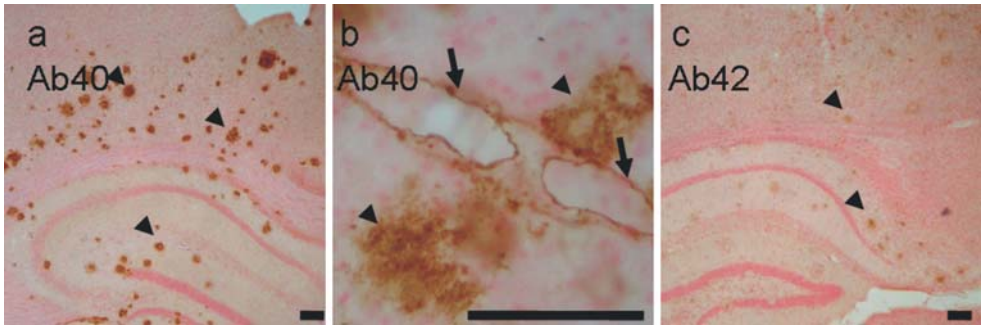

Fig. 8 Immunohistochemistry to detect Aβ using dedicated antibodies showed that amyloid deposits (in both plaques and blood vessels) were mainly formed by Aβ 40 peptides (**a**: low magnification photograph showing Aβ 40 plaques in the isocortex and hippocampus of an old APPxPS1 mouse (*arrow heads*); **b**: high magnification of blood vessels (*arrows*) and amyloid plaques (*arrow heads*) stained with anti-Aβ 40 antibody). **c** On the contrary, Aβ 42 immunostainings were only associated with faint labeling of plaques (*arrow heads*); almost no vascular staining was obtained with Aβ 42 antibodies. Scale bars: 50 μm

APP/PS1 mice, the onset of amyloid deposition in extracellular plaques and in blood vessels is similar to what is found in other aggressive models of AD such as the APPswe/PS1dE9 mice [10]. Some other aggressive mouse models of AD such as the APPswe/PS1(A246E) line however do not show vascular amyloid deposition before the age of 16 months, after the appearance of parenchymal amyloid deposition at the age of 9–13 months [32]. As expected, cerebrovascular amyloid deposition occurs earlier in the APP/PS1 model than in single transgenics such as the APP23 model in which substantial vascular amyloid accumulation starts around 12 months onwards after the appearance of amyloid plaques [11,33,34]. In other single transgenics, despite parenchymal amyloid deposition onset between 8 months (PDAPP model [35]) and 9–12 months (Tg2576 model [35]), CAA appearance seems to be more variable (21 months for PDAPP [36], 10 months for Tg2576 [37,38]).

In our model, amyloid deposition in plaques increased linearly with aging, while CAA development was described by a logarithmic function and seemed to be stabilized beyond 40 weeks. This suggests, despite similar onset, differences between the kinetics of parenchymal and vascular Aβ deposition.

The second part of our study was dedicated to the in vivo characterization of cerebrovasculature of the APP/PS1 mice by using two MRA methods. TOF-MRA, a flow-dependent technique, is very sensitive to blood flow abnormalities. CE-MRA, the second technique, is based on contrast agent-mediated T1 shortening within vessels. As it does not require high flow rate, vessels with low flow rate or turbulent flow can be visualized [39,40]. This may explain why the length of the vessels measured on CE-MRA, for a given genotype and age group, was systematically greater than for TOF-MRA. As a specific example, Fig. 6 shows a greater part of the MCA detected on CE- than on TOF- angiograms. Particularly, on the left side of the images, the distal part of the MCA 'truncated' on the TOF-angiogram (a, arrow) was detected after injection of P792 (b, arrow). This suggests that the signal absence detected on the TOF-angiogram was not related to vessel disruption or loss. As TOF and CE-angiograms were acquired with different parameters, one can argue that "truncated" appearance on TOF-angiograms was due to a slightly different performance of gradients in both acquisitions. However, in the current example, the right side of the MCA was not "truncated" on TOF-angiograms. Altered performance of the gradients can thus not be used to explain truncation effects in the vessels on TOF images.

TOF- and CE-MRA revealed more vessel voids and a reduced vessel length in old APP/PS1 mice with respect to adult ones. Such alterations were not detected in PS1 mice (except for a reduced length of the MCA in aged PS1 mice on CE-angiograms). Brain functional studies of transgenic mouse models of AD have already reported several cerebrovascular abnormalities by using laser Doppler methods. For example, key regulatory mechanisms, such as the endothelium-dependent relaxation, functional hyperemia and cerebrovascular autoregulation are altered in these mice [41–43]. The alterations of the MCA we detected in aged APP/PS1 mice show that vascular alterations can also be detected in vivo at a macroscopic level on TOF- and CE-angiograms. These results are also consistent with previously published in vivo MRA studies focusing on APP23 mouse model of AD [14]. Indeed, these mice also showed angiogram alterations that increased with age. Eleven-month-old APP23 mice showed signal voids at the level of the internal carotid artery. Additional alterations were observed at 20 months at the level of the anterior, middle and posterior cerebral arteries. Interestingly, our results also remind some of the vascular anomalies detected in patients with AD. Indeed, these patients show stenoses at the level of the MCA as well as MCA watershed dominant hypoperfusion [7] and decreased blood velocity [5,6].

The alterations detected on TOF-angiograms might be caused by subtle vessel morphological alterations

(narrowing, compression, partial obliteration…) or decreased vessel elasticity [14,44] leading to flow perturbations. Our studies showed that when a localized void of a vessel was detected on a TOF-angiogram, then, in 77% of the cases it was also detected on the corresponding CE-angiogram. This suggests that most of the alterations found on TOF-angiograms were mainly due to focal morphological alterations of the vessels, big enough to reduce signal intensity beneath detection limit on CE-angiograms. This conclusion is consistent with data presented by Beckmann et al, who showed, by using a corrosion cast method, that altered perfusion detected on TOF-angiograms can be related to morphological anomalies of the vessels such as constrictions or narrowings [14].

The origin of blood vessel alterations remains to be firmly identified. The two age-groups we studied (16–23 weeks versus 60.5–84.5 weeks) displayed different amounts of CAA (from no or few vascular deposits to florid CAA) as shown by our histological study. In a recent publication [45], Thal et al. showed that CAA-related capillary occlusion in the branches of the thalamoperforating arteries of APP23 mice corresponded to the occurrence of blood flow disturbances in MR angiograms. Because amyloid angiopathy was present within the middle cerebral artery that displayed alterations on angiograms, one can expect a causative role of CAA on the alterations we described. Conversely, recent studies have shown that, besides CAA, other histological alterations can modify vessels morphology and function in AD mouse models. For instance, small amyloid deposits peripheral to the vessels but not forming CAA appear to be deleterious [46]. Also, it is strongly suggested that pre-aggregated Aβ species, which have known neurotoxic actions [47] can promote negative effects at the level of brain vasculature: first, vascular abnormalities, including loss of endothelial cells, can be observed in amyloid-free vessels from AD Tg mice, at distance of aggregated Aβ deposits [30]; second, it has been demonstrated that vascular impairments can be detected in young pre-CAA Tg2576 mice [48]; third, there are direct evidence showing that treatment with non-aggregated Aβ modifies vessels architecture (eg endothelial destruction) and function (eg vasoconstriction potentiation [49–51]). These data thus suggest that biological parameters other than CAA can lead to vessel alterations. Finally, the case of the pterygopalatine artery displaying signal voids caused by susceptibility effects illustrates that there might also be different artifacts leading to 'apparently abnormal' flow patterns. For example, iron deposition in the vicinity of the CAA or in amyloid plaques close to the vessels might lead to such artifacts. However, in previous articles, we studied iron depositions in the cortex of our transgenic mice and did not detect severe iron depositions [20,29,52]. Therefore, a contribution of local iron-related susceptibility effects to the signal voids detected in the vessels is unlikely in this model.

Conclusion

In conclusion, cerebrovascular alterations of APP/PS1 mouse model of AD were studied by histology and in vivo MRA. Histology showed cerebrovascular amyloid deposition that started by the same time as extracellular amyloid deposition. CAA increased with age and seemed to be stabilized beyond 40 weeks. In vivo MRA before and after administration of a contrast agent showed vessel alterations at the level of intracerebral vessels. An age-related alteration was detected at the level of the MCA on both TOF- and CE-MRA in aged APP/PS1 mice. These results show that macroscopic vascular abnormalities are part of the pathological alterations developed by APP/PS1 mouse models of AD.

Acknowledgments We thank Sanofi-Aventis Neurodegenerative Disease Group for providing the animals involved in this study. We acknowledge Guerbet research group for the generous gift of the contrast agents used in our study. We thank Dr. Cédric Messaoudi from U759 Inserm/Institut Curie for his help with ImageJ. This work was supported by the Fédération pour la Recherche sur le Cerveau 2003, the Del Duca Foundation, and the ACI Neurosciences 2004 (French Research Department).

References

1. Vinters HV (1987) Cerebral amyloid angiopathy. Crit Rev Stroke 18:311–324
2. Weller RO, Nicoll JA (2003) Cerebral amyloid angiopathy: pathogenesis and effects on the ageing and Alzheimer brain. Neurol Res 25:611–616
3. De la Torre JC (2004) Is Alzheimer's disease a neurodegenerative or a vascular disorder? Data, dogma, and dialectics. Lancet Neurol 3:184–190
4. De la Torre JC (2002) Alzheimer disease as a vascular disorder: nosological evidence. Stroke 33:1152–1162
5. Franceschi M, Alberoni M, Bressi S et al (1995) Correlations between cognitive impairment, middle cerebral artery flow velocity and cortical glucose metabolism in the early phase of Alzheimer's disease. Dement 6:32–38
6. Bressi S, Volonte MA, Alberoni M et al (1992) Transcranial doppler sonography in the early phase of Alzheimers-disease. Dement 3:25–31
7. Ishibashi K, Tanaka K, Nakabayashi T et al (1998) Latent cerebral artery stenoses on magnetic resonance angiography in a patient diagnosed as probable Alzheimer disease. Psychiatr Clin Neurosci 52:93–96
8. Yamada M (2000) Cerebral amyloid angiopathy: an overview. Neuropathol 20:8–22
9. Duyckaerts C, Potier MC, Delatour B (2008) Alzheimer disease models and human neuropathology: similarities and differences. Acta Neuropathol 115:5–38
10. Garcia-Alloza M, Robbins EM, Zhang-Nunes SX et al (2006) Characterization of amyloid deposition in the APPswe/PS1dE9 mouse model of Alzheimer disease. Neurobiol Dis 24:516–524
11. Calhoun ME, Burgermeister P, Phinney AL et al (1999) Neuronal overexpression of mutant amyloid precursor protein results in prominent deposition of cerebrovascular amyloid. Proc Natl Acad Sci USA 96:14088–14093
12. Blanchard V, Moussaoui S, Czech C et al (2003) Time sequence of maturation of dystrophic neurites associated with Ab deposits in APP/PS1 transgenic mice. Exp Neurol 184:247–263

13. Delatour B, Guegan M, Volk A et al (2006) In vivo MRI and histological evaluation of brain atrophy in APP/PS1 transgenic mice. Neurobiol Aging 27:835–847
14. Beckmann N, Schuler A, Mueggler T et al (2003) Age-dependent cerebrovascular abnormalities and blood flow disturbances in APP23 mice modeling Alzheimer's disease. J Neurosci 23:8453–8459
15. Reese T, Bochelen D, Sauter A et al (1999) Magnetic resonance angiography of the rat cerebrovascular system without the use of contrast agents. NMR Biomed 12:189–196
16. Beckmann N, Stirnimann R, Bochelen D (1999) High-resolution magnetic resonance angiography of the mouse brain: application to murine focal cerebral ischemia models. J Magn Reson 140:442–450
17. Penet MF, Viola A, Confort-Gouny S et al (2005) Imaging experimental cerebral malaria in vivo: significant role of ischemic brain edema. J Neurosci 25:7352–7358
18. Wirths O, Multhaup G, Czech C et al (2001) Intraneuronal Abeta accumulation precedes plaque formation in beta-amyloid precursor protein and presenilin-1 double-transgenic mice. Neurosci Lett 306:116–120
19. Wirths O, Multhaup G, Czech C et al (2001) Reelin in plaques of beta-amyloid precursor protein and presenilin-1 double-transgenic mice. Neurosci Lett 316:145–148
20. El Tannir El Tayara N, Delatour B, Le Cudennec C et al (2006) Age-related evolution of amyloid burden, iron load, and MR relaxation times in a transgenic mouse model of Alzheimer's disease. Neurobiol Dis 22:199–208
21. Puchtler H, Sweat F, Levine M (1962) On the binding of Congo red by amyloid. J Histochem Cytochem 10:355–364
22. Tian J, Shi J, Bailey K et al (2003) Negative association between amyloid plaques and cerebral amyloid angiopathy in Alzheimer's disease. Neurosci Lett 352:137–140
23. Tian J, Shi J, Bailey K et al (2004) Relationships between arteriosclerosis, cerebral amyloid angiopathy and myelin loss from cerebral cortical white matter in Alzheimer's disease. Neuropathol Appl Neurobiol 30:46–56
24. Ma B, Zimmermann T, Rohde M et al (2007) Use of autostitch for automatic stitching of microscope images. Micron 38:492–499
25. Port M, Corot C, Rousseaux O et al (2001) P792: a rapid clearance blood pool agent for magnetic resonance imaging: preliminary results. Magn Reson Mater Phy 12:121–127
26. Dorr A, Sled JG, Kabani N (2007) Three-dimensional cerebral vasculature of the CBA mouse brain: a magnetic resonance imaging and micro computed tomography study. NeuroImage 35:1409–1423
27. Scremin OU (2004) Cerebral vascular system. In: The rat nervous system, 3rd edn. Elsevier, Amsterdam, Boston, pp 1167–1202
28. Beckmann N (2000) High resolution magnetic resonance angiography non-invasively reveals mouse strain differences in the cerebrovascular anatomy in vivo. Magn Reson Med 44:252–258
29. El Tannir El Tayara N, Volk A, Dhenain M et al (2007) Transversal relaxation time reflects brain amyloidosis in young APP/PS1 transgenic mice. Magn Reson Med 58:179–184
30. Kumar-Singh S, Pirici D, McGowan E et al (2005) Dense-core plaques in Tg2576 and PSAPP mouse models of Alzheimer's disease are centered on vessel walls. Am J Pathol 167:527–543
31. Kumar-Singh S (2008) Cerebral amyloid angiopathy: pathogenetic mechanisms and link to dense amyloid plaques. Genes Brain Behav 7(Suppl 1):67–82
32. Liu L, Herukka SK, Minkeviciene R et al (2004) Longitudinal observation on CSF Abeta42 levels in young to middle-aged amyloid precursor protein/presenilin-1 doubly transgenic mice. Neurobiol Dis 17:516–523
33. Sturchler-Pierrat C, Abramowski D, Duke M et al (1997) Two amyloid precursor protein transgenic mouse models with Alzheimer disease-like pathology. Proc Natl Acad Sci USA 94:13287–13292
34. Winkler DT, Bondolfi L, Herzig MC et al (2001) Spontaneous hemorrhagic stroke in a mouse model of cerebral amyloid angiopathy. J Neurosci 21:1619–1627
35. Higgins GA, Jacobsen H (2003) Transgenic mouse models of Alzheimer's disease: phenotype and application. Behav Pharmacol 14:419–438
36. Racke MM, Boone LI, Hepburn DL et al (2005) Exacerbation of cerebral amyloid angiopathy-associated microhemorrhage in amyloid precursor protein transgenic mice by immunotherapy is dependent on antibody recognition of deposited forms of amyloid beta. J Neurosci 25:629–636
37. Christie R, Yamada M, Moskowitz M et al (2001) Structural and functional disruption of vascular smooth muscle cells in a transgenic mouse model of amyloid angiopathy. Am J Pathol 158:1065–1071
38. Domnitz SB, Robbins EM, Hoang AW et al (2005) Progression of cerebral amyloid angiopathy in transgenic mouse models of Alzheimer disease. J Neuropathol Exp Neurol 64:588–594
39. Prince MR (1994) Gadolinium-enhanced MR aortography. Radiol 191:155–164
40. Bosmans H, Marchal G, Lukito G et al (1995) Time-of-flight MR angiography of the brain: comparison of acquisition techniques in healthy volunteers. Am J Roentgenol 164:161–167
41. Iadecola C, Zhang F, Niwa K et al (1999) SOD1 rescues cerebral endothelial dysfunction in mice overexpressing amyloid precursor protein. Nat Neurosci 2:157–161
42. Niwa K, Younkin L, Ebeling C et al (2000) Abeta 1-40-related reduction in functional hyperemia in mouse neocortex during somatosensory activation. Proc Natl Acad Sci USA 97:9735–9740
43. Niwa K, Kazama K, Younkin L et al (2002) Cerebrovascular autoregulation is profoundly impaired in mice overexpressing amyloid precursor protein. Am J Physiol Heart Circ Physiol 283:H315–323
44. Krucker T, Schuler A, Meyer EP et al (2004) Magnetic resonance angiography and vascular corrosion casting as tools in biomedical research: application to transgenic mice modeling Alzheimer's disease. Neurol Res 26:507–516
45. Thal DR, Capetillo-Zarate E, Larionov S et al (2009) Capillary cerebral amyloid angiopathy is associated with vessel occlusion and cerebral blood flow disturbances. Neurobiol Aging 30(12):1936–1948
46. Meyer EP, Ulmann-Schuler A, Staufenbiel M et al (2008) Altered morphology and 3D architecture of brain vasculature in a mouse model for Alzheimer's disease. Proc Natl Acad Sci USA 105:3587–3592
47. Selkoe DJ (2008) Soluble oligomers of the amyloid beta-protein impair synaptic plasticity and behavior. Behav Brain Res 192:106–113
48. Han BH, Zhou ML, Abousaleh F et al (2008) Cerebrovascular dysfunction in amyloid precursor protein transgenic mice: contribution of soluble and insoluble amyloid-beta peptide, partial restoration via gamma-secretase inhibition. J Neurosci 28:13542–13550
49. Niwa K, Porter VA, Kazama K et al (2001) A beta-peptides enhance vasoconstriction in cerebral circulation. Am J Physiol Heart Circ Physiol 281:H2417–2424
50. Price JM, Sutton ET, Hellermann A et al (1997) beta-Amyloid induces cerebrovascular endothelial dysfunction in the rat brain. Neurol Res 19:534–538
51. Townsend KP, Obregon D, Quadros A et al (2002) Proinflammatory and vasoactive effects of Abeta in the cerebrovasculature. Ann NY Acad Sci 977:65–76
52. Dhenain M, El Tannir El Tayara N, Wu TD et al (2009) Characterization of in vivo MRI detectable thalamic amyloid plaques from APP/PS1 mice. Neurobiol Aging 30:41–53